Cavitation Bubble Dynamics inside Liquid Drops in Microgravity

D. Obreschkow,[1,2] P. Kobel,[1,3] N. Dorsaz,[1,4] A. de Bosset,[1] C. Nicollier,[5] and M. Farhat[1]

[1]*Laboratoire des Machines Hydrauliques, EPFL, 1007 Lausanne, Switzerland*
[2]*Physics Department, Oxford University, Oxford, OX1 3PU, United Kingdom*
[3]*Max Planck Institute for Solar System Research, 37191 Katlenburg-Lindau, Germany*
[4]*Institut Romand de Recherche Numérique en Physique des Matériaux, EPFL, 1015 Lausanne, Switzerland*
[5]*ESA European Astronaut Centre, Cologne, Germany, and NASA Johnson Space Center, Houston, Texas, USA*

(Received 16 April 2006; published 1 September 2006)

We studied spark-generated cavitation bubbles inside water drops produced in microgravity. High-speed visualizations disclosed unique effects of the spherical and nearly isolated liquid volume. In particular, (1) toroidally collapsing bubbles generate two liquid jets escaping from the drop, and the ''splash jet'' discloses a remarkable broadening. (2) Shock waves induce a strong form of secondary cavitation due to the particular shock wave confinement. This feature offers a novel way to estimate integral shock wave energies in isolated volumes. (3) Bubble lifetimes in drops are shorter than in extended volumes in remarkable agreement with herein derived corrective terms for the Rayleigh-Plesset equation.

DOI: 10.1103/PhysRevLett.97.094502 PACS numbers: 47.55.dp

Introduction.—Hydrodynamic cavitation is a major source of erosion damage in many industrial systems, such as fast ship propellers, cryogenic pumps, pipelines, and turbines [1]. Yet, controlled cavitation-erosion proves a powerful tool for modern technologies like ultrasonic cleaning [2], effective salmonella destruction [3], and treatment for kidney stones [4]. Such erosion is associated with liquid jets and shock waves emitted by collapsing cavitation bubbles, but the relative importance of these two processes remains a topic of debate [5]. Fundamental understanding requires studies of single bubbles in different liquid geometries, since bubble dynamics strongly depends on nearby surfaces by means of boundary conditions imposed on the surrounding pressure field [1,6]. Recent investigations revealed interesting characteristics of bubbles collapsing next to flat [7] and curved [8] rigid surfaces or flat free surfaces [9,10]. It is thus a promising idea to study bubbles inside spherical drops and probe their interaction with closed spherical free surfaces. However, for centimeter-sized volumes, such geometries are inaccessible in the presence of gravity and require a microgravity environment, even though gravity plays a negligible direct role for most single bubble phenomena.

In this Letter, we present the first experimental study of single bubble dynamics inside centimetric quasispherical water drops produced in microgravity. High-speed imaging revealed key implications of nearly isolated, finite, and spherical liquid volumes on bubble evolution and subsequent phenomena. The results will be presented in three steps covering (1) jet dynamics, (2) shock wave effects, and (3) spherical collapse.

Experimental setup [for a detailed description and figures, see [11]].—Microgravity was achieved in manned parabolic flights conducted by the European Space Agency ESA (42nd parabolic flight campaign). The nominal flight manoeuvres offer sequences (i.e., parabolas) of 20 s of weightlessness with a residual g-jitter of 0.02–0.05 g at typical frequencies of 1–10 Hz. Our experiment and all calibrations were carried out on 93 parabolas on three consecutive flight days.

Each parabola was used to run one fully automated experimental cycle, consisting in the computer-controlled growth of a centimetric water drop and the generation of a single bubble inside the drop. The liquid was expelled through an injector tube, specially designed to fix and stabilize the ensuing truncated drop (Fig. 1). The bubble was generated through a spark discharge between two thin electrodes immersed in the drop. A high-speed CCD camera (Photron Ultima APX, up to 120 000 frames/s) recorded the fast bubble dynamics for a sequence of 11 ms. Three parameters were independently adjustable: (1) the initial drop size (radius $R_{d,\min} = 8$–13 mm) by changing the expelled water volume, (2) the maximal bubble size (radius $R_{b,\max} = 2$–10 mm) by altering the discharge energy between 8 and 1000 mJ, (3) the distance d between

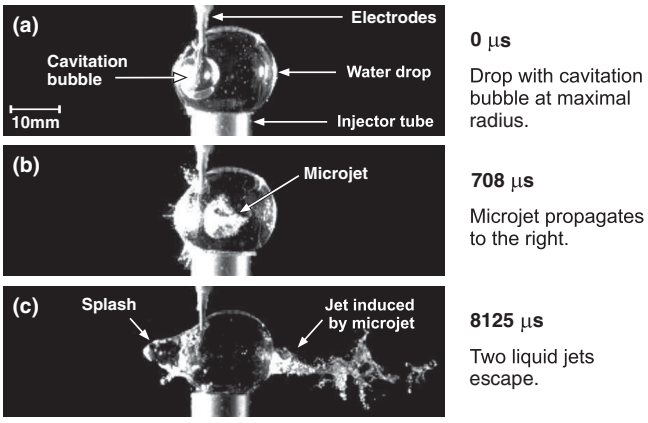

FIG. 1. Two liquid jets generated by the toroidal implosion of a cavitation bubble ($\alpha = 0.3$, $\varepsilon = 0.45$). Movies at [11].

drop center and bubble center by precisely adjusting the electrodes position. We shall usually describe a particular setting in the dimensionless parameter space (α, ε), where $\alpha \equiv R_{b,\max}/R_{d,\min}$ (relative bubble radius), $\varepsilon \equiv d/R_{d,\min}$ (eccentricity).

Jet dynamics.—As a first result, we overview the collapse of eccentrically placed cavitation bubbles in the parameter range ($0.2 < \alpha < 0.6$, $0.3 < \varepsilon < 0.8$), recorded at 24 000 frames/s (extracts in Fig. 1). The nearby free surface breaks the spherical symmetry leading to a toroidal implosion [9] with a fast microjet (>50 m/s) directed perpendicularly away from the closest surface element [Fig. 1(b)]. This microjet accelerates the surrounding volume forming a jet that escapes from the right surface in the figure at a reduced velocity (6 m/s). In the meantime, a slower splash escapes in the opposite direction [Fig. 1(c)]. This double-jet picture is consistent with established studies of bubbles in the vicinity of free surfaces [9,12], and provides the first direct visualization of both bubble-induced jets escaping from a steady liquid volume.

Close investigation of the splash geometry revealed a remarkable and reproducible diameter broadening compared to similar jets on ground-based flat free surfaces [Fig. 2(a) and 2(c)]. In the latter case, the narrowness is due to a very localized high-pressure peak between bubble and free surface [9]. We believe that this pressure peak is much broader beneath spherical free surfaces, since the distance between bubble boundary and surface varies more smoothly. Such a pressure zone broadening suggests an explanation for a broader splash and will be subject to forthcoming simulations. Additionally, we discovered that the typical crown surrounding the splash on flat surfaces [Fig. 2(c)] is absent on the spherical surface [Fig. 2(a)]. For comparison it is enlightening to consider cylindrical free surfaces, which are straight and circular in two orthogonal directions. One might reason that such surfaces exhibit a hybrid behavior between (a) and (c). Indeed, recent studies of bubbles inside a falling water stream [13] revealed a noncircular crown consisting of two spikes in the straight direction of the surface, while no crown seems present perpendicular to the figure [Fig. 2(b)]. These observations definitely disclose nontrivial features in splash dynamics and crown formation and promise an interesting avenue for future research.

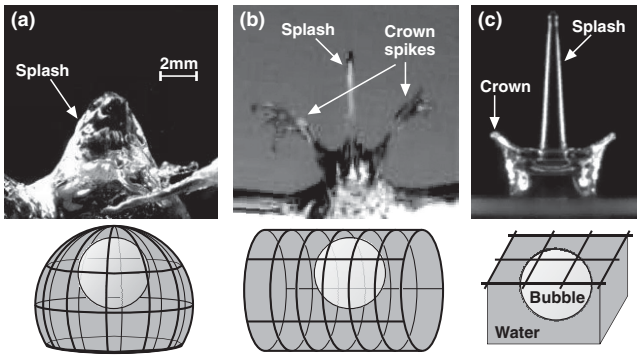

FIG. 2. Splash on several free surfaces. [On (a), electrodes enter from the right. (b) was provided by Robert [13].]

Shock wave effects.—Many high-speed visualizations contain isolated frames showing a short-lived brilliant mist (Fig. 3). This mist lasts for roughly 50 μs and is visibly composed of submillimetric bubbles (here called microbubbles). Strikingly, these mists exactly coincide with the instants of predicted shock wave radiation. Namely, the spark (or primary) shock wave is emitted at the spark generation initiating the bubble growth, and collapse (or secondary) shock waves are radiated at the bubble collapse and subsequent collapses of rebound bubbles [14]. Although these shock waves were not directly observable with the present setup, their exact synchronization with microbubbles clearly discloses a causal relation. We claim that the mist of microbubbles is a strong form of shock wave-induced secondary cavitation [15]. In other words, microbubbles are small cavitation bubbles inside the drop volume, arising from the excitation of nuclei (i.e., microscopic impurities and dissolved gas) at the passage of shock waves [16,17]. That the microbubbles were indeed cavities was confirmed by showing that their size-lifetime ratio matches theoretical cavity life cycles.

The surprisingly high abundance of microbubbles compared to faint traces seen in ground experiments [15] is reasonably explained by a unique shock wave confinement in the case of isolated liquid volumes. The shock wave can be reflected many times on the free surface and thereby transfer its whole energy to microbubbles via multiple excitations. This full energy transformation offers a new way to estimate integral shock wave energies. The idea consists in integrating the energies of all microbubbles, which can be inferred from statistical measures of their densities and maximal volumes $V_{\max}$ via $E = V_{\max}(p_\infty - p_V)$ [18], where p_∞ is the ambient static pressure and p_V is the vapor pressure. Applying this method to five concrete samples showed that 50%–70% of the initial electrical energy (200 mJ) is contained in the mist of microbubbles associated with the spark shock. It follows that 50%–70% of the spark energy is radiated in a shock wave, and we expect to find the remaining 30%–50% in the main bubble, a prediction which is consistent with the measured maximal main bubble volume corresponding to a bubble energy

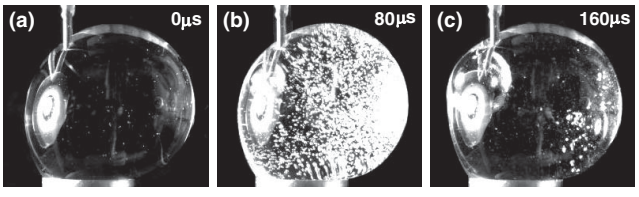

FIG. 3. Example of secondary cavitation: the primary shock wave radiated between (a) and (b) induces a short-lived mist of microbubbles. Movies at [11].

of 70 mJ. The actual precision was limited by the optical resolution and nonvanishing contact surfaces (injector tube, electrodes), and could be improved in forthcoming studies.

Spherical collapse.—We shall now investigate the collapse of bubbles centered in drops ($\varepsilon = 0$), since their spherical symmetry allows a direct comparison to bubbles in infinite volumes, governed by the Rayleigh-Plesset theory [18,19]. Bubbles in drops were found to collapse faster in excellent agreement with a theoretical extension derived in the following. Note that gravity does not play a direct role in Rayleigh-Plesset's theory, nor in our extension, but its absence allowed the realization of isolated drops with centimetric diameters.

In the present approach we neglect surface tension, liquid compressibility, viscosity, and mass transfer across the bubble boundary. We further assume a uniform and constant temperature, and take the pressure inside the bubble as the vapor pressure p_V. The ensuing simplified Rayleigh(-Plesset) equation for a spherical bubble with radius $R_b(t)$ in an infinite liquid reads

$$\frac{-\Delta p}{\rho} = \frac{3}{2}\dot{R}_b{}^2 + R_b\ddot{R}_b, \tag{1}$$

where ρ is the liquid density and $\Delta p \equiv p_\infty - p_V$ with p_∞ being the liquid pressure taken far from the bubble. Integrating (1) provided the initial conditions $R_b(0) = R_{b,\max}$ and $\dot{R}_b(0) = 0$ yields the radius $R_b(t)$ of the collapsing bubble. The so-called Rayleigh collapse time T_{Rayl}, such that $R_b(T_{\text{Rayl}}) = 0$, is given by $T_{\text{Rayl}} \approx 0.915 R_{b,\max}\sqrt{\rho/\Delta p}$ [18]. To compare different bubble collapses, we present their functions $R_b(t)$ in normalized scales where T_{Rayl} and $R_{b,\max}$ equal one. In these scales, $R_b(t)$ can be shown to be independent of Δp, ρ, and $R_{b,\max}$. To assert the validity of the above model for the present situation, we carried out extensive ground studies with millimetric bubbles in extended water volumes. The data revealed excellent agreement with the theoretical prediction (Fig. 4, dashed line and squares), thus justifying the above assumptions.

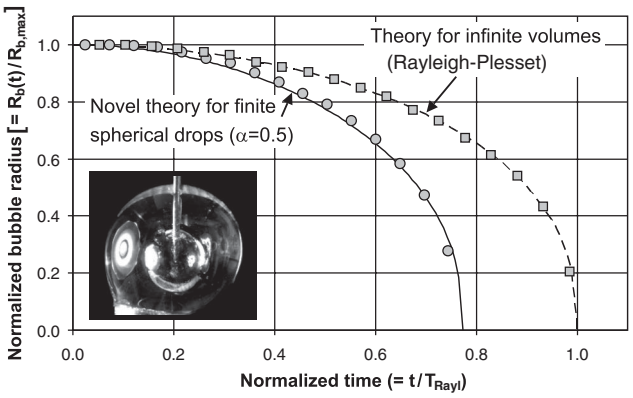

FIG. 4. Bubble collapse. (dashed line) Rayleigh-Plesset theory (1). (squares) Ground-experiment in extended water volumes. (solid line) Modified theory for spherical drops, $\alpha = 0.5$ (5). (circles) Microgravity experiment in drops. Errors are given by the size of the data points.

In microgravity, we studied bubbles centered in drops with a relative radius $\alpha = 0.50$ ($R_{b,\max} = 4.07$ mm, $R_{d,\min} = 8.15$ mm, cabin pressure $p_\infty = 80000$ Pa, spark energy = 200 mJ). The bubble collapses were sampled at 50 000 frames/s with an optical resolution of 70 μm. Given this high spatiotemporal resolution, the results from 5 experimental runs were indistinguishable and ensured reproducibility. The collapse time was measured as 330 ± 10 μs and the evolving bubble radius $R_b(t)$ was reconstituted from the images using a model of optical refraction by a water sphere [11]. Plotted in normalized scales, the microgravity data reveal a remarkable shortening of the collapse time (Fig. 4, circles).

In order to explain this shortening, we shall now derive an equation of motion for cavitation bubbles of radius $R_b(t)$ centered in spherical drops of radius $R_d(t)$, using the above assumptions. Incompressibility links $R_b(t)$ and $R_d(t)$ and conditions the radial velocity $\dot{r}$, as seen by integrating $\nabla \cdot \vec{v} = 0$ along a radial axis,

$$R_d(t) = [R_{d,\min}^3 + R_b^3(t)]^{1/3} \tag{2}$$

$$\dot{r} = \dot{R}_b R_b^2/r^2. \tag{3}$$

For the sake of physical interpretation, we derive the equation of motion from energy conservation. The kinetic energy results from integrating the energy density $\frac{1}{2}\rho\dot{r}^2$ over the whole liquid volume and the potential energy is given by integrating the pressure work pdV over the volume traversed by the bubble surface and the drop surface. Using (2) and (3),

$$E_{\text{kin}} = 2\pi\rho\dot{R}_b^2 R_b^3(1-\lambda), \qquad E_{\text{pot}} = \frac{4\pi R_b^3}{3}\Delta p \tag{4}$$

with $\lambda(t) \equiv R_b(t)/R_d(t)$. Invoking the conservation law $\dot{E}_{\text{kin}} + \dot{E}_{\text{pot}} = 0$ and dividing by $4\pi\rho\dot{R}_b R_b^2$ yields the equation of motion for bubbles centered in drops,

$$\frac{-\Delta p}{\rho} = \frac{3}{2}\dot{R}_b^2 + R_b\ddot{R}_b - 2\dot{R}_b^2\lambda - R_b\ddot{R}_b\lambda + \frac{1}{2}\dot{R}_b^2\lambda^4, \tag{5}$$

where the term in λ^4 was obtained by substituting $\dot{R}_d$ using relation (2). This equation comprises the simplified Rayleigh-Plesset equation (1) and three novel corrective terms, which vanish as $R_d \to \infty$. Up to the factor $4\pi\rho\dot{R}_b R_b^2$ the two terms in λ subtract the change of kinetic energy associated with the volume outside the drop ($R_d(t) < r < \infty$), which needs to be removed from the infinite medium of Rayleigh's model. The remaining corrective term in λ^4 accounts for the change in kinetic energy due to the variation of the drop's radius. This term becomes negligible for relative bubble radii $\alpha \ll 1$ since $\lambda(t) < \alpha \forall t$. Integrating (5) with the initial conditions $R_b(0) = R_{b,\max}$ and

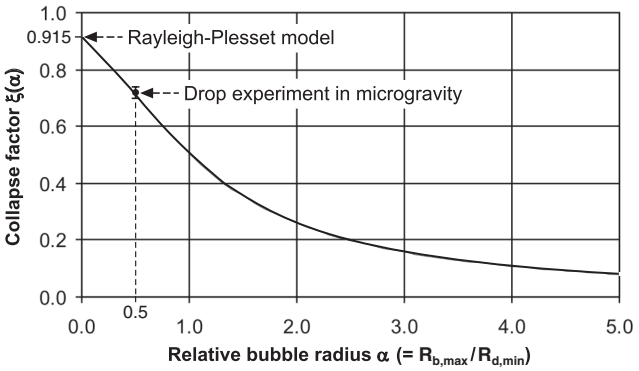

FIG. 5. Collapse factor $\xi(\alpha)$ as a function of the relative bubble radius α. $\xi(\alpha)$ is directly proportional to the collapse time T_{collapse} if ρ, Δp, and $R_{b,\max}$ are fixed.

$\dot{R}_b(0) = 0$ gives the collapsing bubble radius $R_b(t)$, which is in excellent agreement with the microgravity data (Fig. 4, solid line). This proves that the shortened lifetime is entirely due to the finite spherical drop volume, and validates the derived equation of motion for bubbles centered in spherical drops (5).

Finally, we apply the validated model to predict the collapse times of bubbles with arbitrary relative radii α. The energy conservation $E_{\text{kin}} + E_{\text{pot}} = E_0$ can be solved for $\dot{R}_b$, if E_0 is identified with the potential energy at maximal bubble radius $R_{b,\max}$,

$$\dot{R}_b = -\sqrt{\frac{1}{1-\lambda}\,\frac{2\Delta p}{3\rho}\left(\frac{R_{b,\max}^3}{R_b^3} - 1\right)}. \tag{6}$$

Integrating this equation from $R_b = R_{b,\max}$ to $R_b = 0$ yields an analytical expression for the collapse time,

$$T_{\text{collapse}} = \xi(\alpha) R_{b,\max}\sqrt{\frac{\rho}{\Delta p}}$$

$$\xi(\alpha) \equiv \sqrt{\frac{3}{2}}\int_0^1 \left(1 - \frac{s}{(\alpha^{-3} + s^3)^{1/3}}\right)^{1/2}\left(\frac{1}{s^3} - 1\right)^{-1/2} ds, \tag{7}$$

where s substitutes $R_b/R_{b,\max}$. The collapse time depends on α through a collapse factor $\xi(\alpha)$ plotted in Fig. 5. For infinite liquids ($\alpha = 0$) we consistently recover the Rayleigh collapse factor $\xi(0) = 0.915$ [18]. $\xi(\alpha)$ decreases monotonically with increasing relative bubble radius α, and tends to 0 for $\alpha \to \infty$. Even though this limit could not be probed in the microgravity time available, it seems nonphysical for it violates the model assumptions. In particular, for $\alpha \gtrsim 6$ the drop's surface velocity $\dot{R}_d(t)$ would approach the speed of sound for a significant fraction of the collapse phase [use (2) and (6)], thus implying a strong pressure drop and preventing further acceleration.

Conclusion.—Microgravity conditions proved essential in the study of cavitation bubbles inside centrimetric water drops. In particular, (1) we obtained the first simultaneous visualizations of both cavity-induced liquid jets, and discovered a remarkable splash broadening and missing crown formation on spherical surfaces. (2) Reflected shock waves led to a strong form of secondary cavitation and offer an original way for the measurement of shock wave energies inside isolated volumes. (3) Our Rayleigh-Plesset-like model for bubbles in drops is in excellent agreement with specific experiments and allowed a general prediction of bubble collapse times in drops. Forthcoming microgravity studies could fruitfully address the limit of large bubble radii ($\alpha \gg 1$), or focus on direct shock wave visualizations.

We thank the ESA for having pursued this research and the Swiss NSF for Grant No. 2000-068320.

[1] C. E. Brennen, *Cavitation and Bubble Dynamics* (Oxford University Press, New York, 1995).
[2] W. D. Song, M. H. Hong, B. Lukyanchuk, and T. C. Chong, J. Appl. Phys. **95**, 2952 (2004).
[3] D. M. Wrigley and N. G. Llorca, Journal of Food Protection **55**, 678 (1992).
[4] W. Sass, M. Braunlich, H. P. Deyer, E. Matura, W. Folberth, H. G. Priemeyer, and J. Seifert, Ultrasound Med. Biol. **17**, 239 (1991).
[5] A. Shima, Shock Waves **7**, 33 (1997).
[6] M. S. Plesset and R. B. Chapman, J. Fluid Mech. **47**, 283 (1971).
[7] E. A. Brujan, G. S. Keen, A. Vogel, and J. R. Blake, Phys. Fluids **14**, 85 (2002).
[8] Y. Tomita, R. B. Robinson, R. P. Tong, and J. R. Blake, J. Fluid Mech. **466**, 259 (2002).
[9] R. B. Robinson, J. R. Blake, T. Kodama, A. Shima, and Y. Tomita, J. Appl. Phys. **89**, 8225 (2001).
[10] A. Pearson, E. Cox, J. R. Blake, and S. R. Otto, Engineering Analysis with Boundary Elements **28**, 295 (2004).
[11] Project site: www.flashandsplash.ch, go to "science".
[12] L. A. Crum, J. Phys. (Paris), Colloq. **40**, 2858 (1979).
[13] E. Robert, MS thesis, École Polytechnique Fédérale de Lausanne, 2004.
[14] T. Kodama and Y. Tomita, Appl. Phys. B **70**, 139 (2000).
[15] Y. Tomita, T. Kodama, and A. Shima, Appl. Phys. Lett. **59**, 274 (1991).
[16] B. Wolfrum, T. Kurz, R. Mettin, and W. Lauterborn, Phys. Fluids **15**, 2916 (2003).
[17] G. N. Sankin, W. N. Simmons, S. L. Zhu, and P. Zhong, Phys. Rev. Lett. **95**, 034501 (2005).
[18] L. Rayleigh, Philos. Mag. **34**, 94 (1917).
[19] M. S. Plesset, J. Appl. Mech. **16**, 277 (1949).